a (10,10) tube on two layers of graphite. A jellium tip and a lower contact were used to simulate the experimental geometry, and the tip contacted the NT along its entire length. The electronic structure of both the graphite and the tube is described with a simple π-orbital tight binding model. *I-V* curves were obtained as discussed previously (*21*) and were fit to the experimental data with a single parameter for the NT-HOPG hopping. Sample calculations were also performed on a MWNT consisting of a (5,5) tube nested inside a (10,10) tube, and no significant differences were observed. The results of our calculations are shown along with the experimental results in Fig. 2B. We found excellent agreement, indicating that the relaxation of the momentum conservation condition (caused here by finite size effects) can account for the angular dependence of $R(\Phi)$. Furthermore, this agreement indicates that our experimental results will scale to single-walled NTs. This is consistent with calculations studying NT-NT contacts (*22, 23*).

Our results indicate the importance of electron momentum conservation at interfaces, particularly for carbon NTs, where the discrete Fermi surface allows states only in specific directions. Our study implies that the relative angle between the lattices of the NTs can produce dramatic effects, and its control can be exploited in the design of electronic devices and actuating systems.

References and Notes

1. P. Delaney, M. Di Ventra, *Appl. Phys. Lett.* **75**, 4028 (1999).
2. J. Tersoff, *Appl. Phys. Lett.* **74**, 2122 (1999).
3. _____, *Appl. Phys. Lett.* **75**, 4030 (1999).
4. J. W. Mintmire, B. I. Dunlap, C. T. White, *Phys. Rev. Lett.* **68**, 631 (1992).
5. V. H. Crespi, M. L. Cohen, A. Rubio, *Phys. Rev. Lett.* **79**, 2093 (1997).
6. M. Bockrath *et al.*, *Nature* **397**, 598 (1999).
7. S. J. Tans, A. R. M. Verschueren, C. Dekker, *Nature* **393**, 49 (1998).
8. Z. Yao, H. W. C. Postma, L. Balents, C. Dekker, *Nature* **402**, 273 (1999).
9. C. Schonenberger, A. Bachtold, C. Strunk, J. P. Salvetat, L. Forro, *Appl. Phys. A Mat. Sci. Process.* **69**, 283 (1999).
10. M. S. Fuhrer *et al.*, *Science* **288**, 494 (2000).
11. M. R. Falvo *et al.*, *Nature* **397**, 236 (1999).
12. M. R. Falvo, J. Steele, R. M. Taylor II, R. Superfine, *Phys. Rev. B* **62**, 10665 (2000).
13. H. Dai, E. W. Wong, C. M. Lieber, *Science* **272**, 523 (1996).
14. A. Bachtold *et al.*, *Phys. Rev. Lett.* **84**, 6082 (2000).
15. A. Bachtold *et al.*, *Nature* **397**, 673 (1999).
16. S. Frank, P. Poncharal, Z. L. Wang, W. A. de Heer, *Science* **280**, 1744 (1998).
17. M. S. Dresselhaus, G. Dresselhaus, P. C. Eklund, *Science of Fullerenes and Carbon Nanotubes* (Academic Press, San Diego, CA, 1996).
18. P. R. Wallace, *Phys. Rev.* **71**, 622 (1947).
19. P. G. Collins, K. Bradley, M. Ishigami, A. Zettl, *Science* **287**, 1801 (2000).
20. M. Kruger, M. R. Buitelaar, T. Nussbaumer, C. Schonenberger, preprint available at http://xxx.lanl.gov/abs/cond-mat/0009171 (2000).
21. M. Buongiorno Nardelli, J. Bernholc, *Phys. Rev. B Condens. Matter* **60**, R16338 (1999).
22. A. Buldum, J. P. Lu, preprint available at http://arXiv.org/ftp/cond-mat/papers/0005/0005523.pdf (2000).
23. A. A. Maarouf, C. L. Kane, E. J. Mele, *Phys. Rev. B* **61**, 11156 (2000).

24. We are grateful to A. Buldum and J. P. Lu for many useful discussions regarding these experiments as well as their own results. Supported by NSF, the Office of Naval Research–Multidisciplinary Research Program of the University Research Initiative, and NIH–National Center for Research Resources.

15 August 2000; accepted 30 October 2000

Formation of Sphalerite (ZnS) Deposits in Natural Biofilms of Sulfate-Reducing Bacteria

Matthias Labrenz,[1] Gregory K. Druschel,[1] Tamara Thomsen-Ebert,[2] Benjamin Gilbert,[3] Susan A. Welch,[1] Kenneth M. Kemner,[4] Graham A. Logan,[5] Roger E. Summons,[5] Gelsomina De Stasio,[3] Philip L. Bond,[1] Barry Lai,[4] Shelly D. Kelly,[4] Jillian F. Banfield[1]*

Abundant, micrometer-scale, spherical aggregates of 2- to 5-nanometer-diameter sphalerite (ZnS) particles formed within natural biofilms dominated by relatively aerotolerant sulfate-reducing bacteria of the family *Desulfobacteriaceae*. The biofilm zinc concentration is about 10^6 times that of associated groundwater (0.09 to 1.1 parts per million zinc). Sphalerite also concentrates arsenic (0.01 weight %) and selenium (0.004 weight %). The almost monomineralic product results from buffering of sulfide concentrations at low values by sphalerite precipitation. These results show how microbes control metal concentrations in groundwater- and wetland-based remediation systems and suggest biological routes for formation of some low-temperature ZnS deposits.

Microbial reduction of sulfate by sulfate-reducing bacteria (SRB) in anoxic environments is the only major source of low-temperature sulfide in natural waters (*1*). Sulfide can react with metals to form insoluble products (*2*). Formation of ZnS by SRB under certain laboratory conditions was demonstrated in the 1950s and 1960s (*3–5*). However, the microbiological, geochemical, and mineralogical interactions leading to ZnS biomineralization in complex natural systems have not been deciphered. Here we report low-temperature, biologically mediated sphalerite precipitation from dilute natural solutions. Microbial precipitation reactions such as those documented here may be central to mine-waste remediation strategies that use natural or artificial wetlands (*1*, *6*). By an analogous process, ancient microorganisms may have contributed to the low-temperature (or early) stages of formation of the large-stratiform sediment-hosted (and other) ZnS ore deposits.

[1]Department of Geology and Geophysics, University of Wisconsin–Madison, 1215 West Dayton Street, Madison, WI 53706, USA. [2]Diversions Scuba, Madison, WI 53705, USA. [3]Department of Physics, University of Wisconsin–Madison, 1150 University Avenue, Madison, WI 53706, USA. [4]Argonne National Laboratory, Argonne, IL 60439, USA. [5]Australian Geological Survey Organisation, GPO Box 378, Canberra ACT 2601, Australia.

*To whom correspondence should be addressed. E-mail: jill@geology.wisc.edu

We studied biofilms collected by SCUBA divers from a flooded tunnel within carbonate rocks that host the Piquette Pb-Zn deposit (Tennyson, Wisconsin). Despite the generation of acid due to dissolution of some remaining sulfide ore, the high carbonate–buffering capacity maintains the pH between ~7.2 and 8.6. The water meets drinking-water standards [<5 ppm Zn (*7*)], and water from nearby wells is used for this purpose (Table 1).

The biofilms are gray [see supplementary material (*8*)] because they lack ferrihydrite and goethite, which are commonly associated with bacteria in more oxidized regions of the tunnel system (*9*). Characterization by optical microscopy, scanning electron microscopy (SEM), and transmission electron microscopy (TEM) (*8*) (Figs. 1 and 2, A to C) revealed that cells are closely associated with spherical mineral aggregates up to 10 μm in diameter (*8*). Energy dispersive x-ray (Fig. 2D), synchrotron-based x-ray photoelectron emission microscopy (PEEM), and x-ray microprobe analyses (*8*) show that aggregates contain abundant Zn and S. Selected area electron diffraction patterns display diffuse powder rings (Fig. 2B). The *d*-values and ring-pattern structure indicate that aggregates consist of randomly oriented, finely crystalline sphalerite (ZnS). High-resolution TEM images reveal that the diameter of particles within aggregates is ~3 nm (*8*). Thus, ~3-μm-diameter aggregates consist of about a

billion ZnS particles [compare with (*10*, *11*)].

The presence of sulfide within cell-associated mineral aggregates was confirmed by synchrotron-based x-ray PEEM. PEEM data also indicated the presence of sulfate. Ca- and S-rich precipitates were detected by analytical TEM. $CaSO_4 \cdot 2(H_2O)$ probably formed from dissolved sulfate when the biofilms were dried.

Synchrotron-based x-ray microprobe analyses indicated that sphalerite contains As and Se, only minor Fe, and no detectable Pb (Table 2). Reduction of arsenate and selenate by sulfate-reducing bacteria has been reported previously (*12*, *13*). Using the Zn Kα x-ray fluorescence intensity (as compared with thin-film glass standards) during interaction of the beam with a spherical 1-μm-diameter aggregate (column [1], Table 2), we determined that the aggregate has about 55% porosity. This is consistent with TEM data, which showed that aggregates were composed of semirandomly packed nanocrystals.

Phylogenetic studies were performed to characterize the biofilm community (*8*). Small-subunit ribosomal RNA (SSU rRNA) gene analyses revealed a high diversity of SRB, all of which belonged to the family *Desulfobacteriaceae* (Fig. 3). SRB clones constituted up to 38% of all bacterial clones. One sulfide-oxidizing species (*Beggiatoa* sp.) was detected. This implies that the biofilm has more oxidized regions and that ZnS precipitation is localized within reduced zones of a layered microbial community. Free fatty acids were also extracted from the biofilm and analyzed [Fig. 4 (*8*)] as their fatty acid methyl ester (FAME) derivatives. The abundant iso and anteiso $C_{15:0}$ along with iso and anteiso $C_{17:0}$ FAMEs are diagnostic of sulfate-reducing bacteria and, more specifically, of *Desulfobacteriaceae* and *Desulfovibrionaceae* (*14*). The 10-methyl $C_{16:0}$ FAME occurs consistently in *Desulfobacter and Desulfobacterium* spp. (*14*).

Fluorescence in situ hybridization (*8*) to individual cells in environmental samples with the gene probe SRB385Db for the family *Desulfobacteriaceae* revealed abundant chains of elongate cells belonging to this family (*8*). Cells that bound this probe were often surrounded by ZnS (Fig. 5). This result

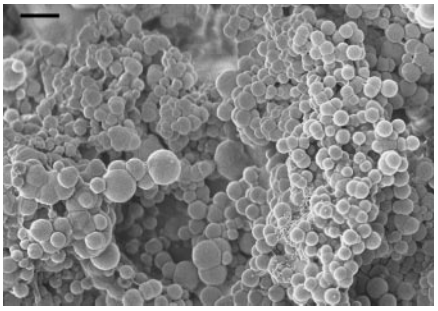

Fig. 1. SEM image of a typical area of the biofilms. Almost the entire biofilm consists of spherical aggregates and associated cells (cells are not evident at this magnification). Bar, 3 μm.

Table 1. Composition of water in the tunnel system and from the biofilm from the Piquette Mine (April 2000) analyzed by ion chromatography. The iron content was close to the detection limit (~1 ppm).

Ion	Tunnel solution (ppm)	Biofilm solution (ppm)
Cl	44.4 ± 2	41.4
NO_3	2.8 ± 0	3.0
SO_4	112.8 ± 14	180
Na	13.7 ± 1	13.2
K	1.8 ± 0	1.9
Mg	56.6 ± 0.5	58.3
Ca	107 ± 2	108
Zn	0.45 ± 0.35	0.24 to 0.95

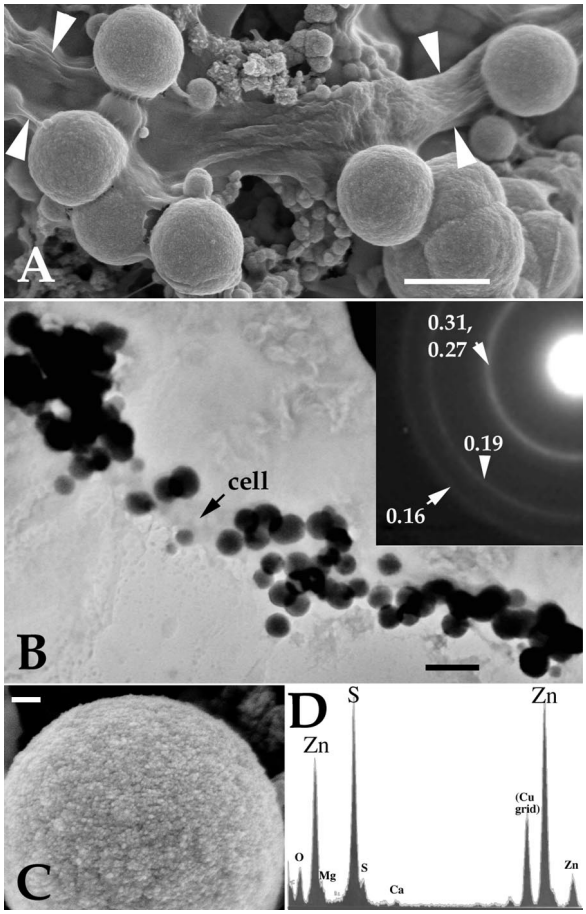

Fig. 2. (**A**) SEM image of a chain of filamentous cells (width indicated by white arrowheads; dehydrated because of the vacuum) and associated micrometer-scale mineral aggregates. Bar, 1 μm. (**B**) TEM image of a chain of cells (low contrast; bar, 1 μm) and aggregates (dark contrast). (**Inset**) Selected area electron diffraction pattern from aggregates with interplanar spacings (in nanometers). (**C**) High-resolution SEM image showing that the aggregates in (A) and (B) consist of few-nanometer-diameter particles (indicated by surface roughness). Bar, 0.1 μm. (**D**) Energy-dispersive x-ray spectrum. Data indicate that micrometer-scale objects are aggregates of randomly oriented, few-nanometer-diameter crystals of sphalerite (ZnS).

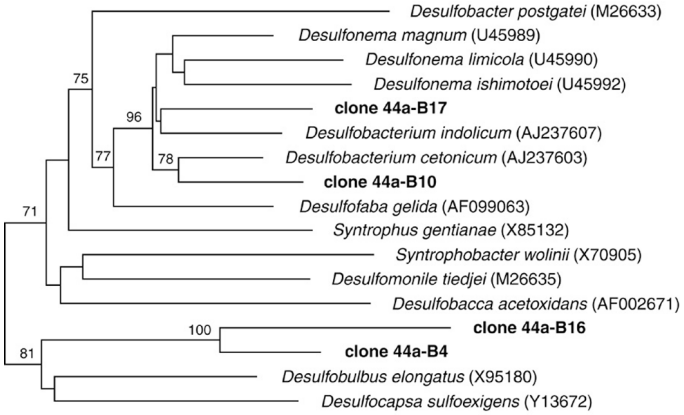

Fig. 3. Phylogenetic relationships of clones 44a-B17, 44a-B10, 44a-B16, and 44a-B4 within the *Desulfobacteriaceae*. The neighbor-joining tree was rooted with *Desulfovibrio desulfuricans* as the outgroup and is based on a comparison of 1229 nucleotides. The branching pattern was tested with 500 bootstrap resamplings, but only those above 70% are shown. Accession numbers are shown for the comparison sequences that were obtained from the GenBank databases. Bar, 0.05 mutation per nucleotide position.

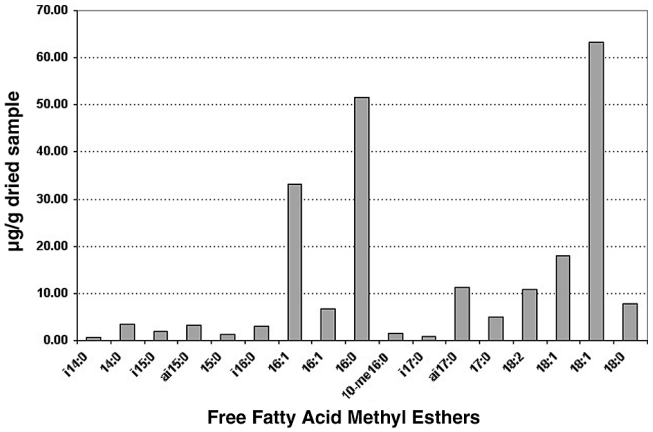

Fig. 4. Free fatty acid methyl ester (FAME) content of the biofilm (micrograms per gram of dried sample). The 16:1 and 18:1 isomers have not been distinguished. The iso (i), anteiso (ai) 15:0 and 17:0, and the 10-methyl FAMEs are distinctive of sulfate-reducing bacteria.

verifies that *Desulfobacteriaceae* are responsible for sphalerite precipitation in the biofilm. As expected on the basis of SSU rRNA gene analysis, *Desulfovibrionaceae* (the other group possibly consistent with the lipid signatures) were not detected with gene probe SRB385. The almost exclusive presence of *Desulfobacteriaceae* in our samples could reflect the nature of the carbon sources. Phylogenetic relatives of our SRB clones (Fig. 3) are able to degrade alkenes or aromatics (*15*).

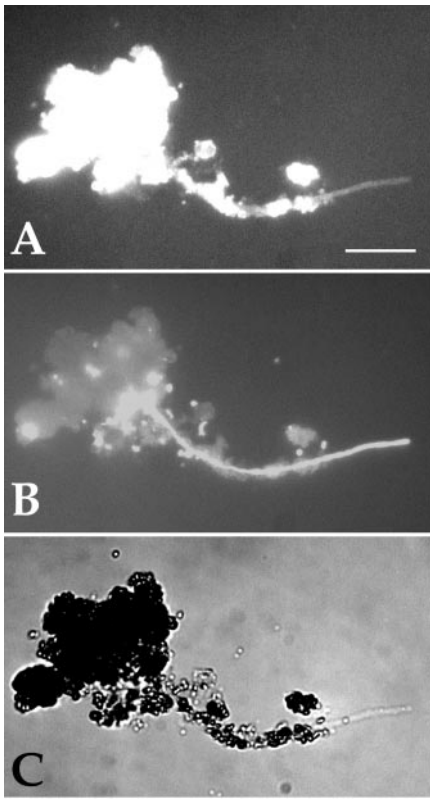

Fig. 5. (**A**) Bacterial cell hybridized with gene probe SRB385Db. The cell is surrounded by highly autofluorescent ZnS granules. Bar, 10 μm. (**B**) Bacterial cell labeled with a stain (DAPI, 4′,6′-diamidino-2-phenylindole) that binds to the DNA of all cells, and (**C**) viewed in plane-polarized light, where mineral aggregates are apparent.

However, appreciable amounts of BTEX (benzene, toluene, ethylbenzene, and xylene) compounds were not detected in solution. The SRB may use organic products of nearby communities of iron-oxidizing autotrophs or surface-derived organic inputs as substrates.

Some *Desulfobacteriaceae* are aerotolerant. This characteristic is associated with *Desulfonema* sp. (Fig. 3) and some of their relatives within the *Desulfobacteriaceae* [e.g., *Desulfobacter* sp. or *Desulfococcus multivorans* (*16*, *17*)]. *Desulfonema* can glide (*18*). Filamentous relatives of *Desulfonema* in our samples may also be motile, allowing them to grow in close proximity to the oxic zone. The ability of the SRB assemblage to grow under only moderately reducing conditions (defined by ZnS precipitation, see below and Fig. 6) is central to our explanation for near exclusive precipitation of sphalerite in our samples.

Geochemical modeling was performed to investigate how microbial processes induce sphalerite precipitation from the groundwater solution. Concentrations of cations and anions (Table 1) were input into the Geochemist's Workbench 3.0 software, and the speciation was calculated at a redox potential appropriate for bulk, relatively oxidized fluid (Eh + 800 mV). The total CO_2 concentration was set at saturation with respect to dolomite [$CaMg(CO_3)_2$], but dolomite precipitation was suppressed to simulate kinetic inhibition. Fluid evolution was modeled by decreasing the solution redox potential to an Eh of −200 mV, simulating the onset of reducing conditions in the biofilm (progressing from left to right in Fig. 6). Sphalerite precipitated at an Eh of −122 to −132 mV (for solutions containing between 1 and 0.1 mg of Zn per liter) and buffered the Eh until Zn^{2+} was consumed. Mackinawite (FeS), and not pyrite, is the expected iron sulfide below 100°C (*19*). When the precipitation of pyrite (FeS_2) was suppressed, solutions became saturated with mackinawite [thermodynamic data of (*19*)] below an Eh of −190 mV (pyrite saturation occurred at an Eh below −151 mV). Precipitation of iron sulfides in the natural open system is not expected. Zn influx by way of slowly moving groundwater solutions (thus, ZnS precipitation) will prevent the sulfide accumulation necessary to achieve an Eh consistent with precipitation of iron sulfides. Removal of sulfide by ZnS formation also prevents the development of highly reducing conditions needed for anaerobic groups of SRB.

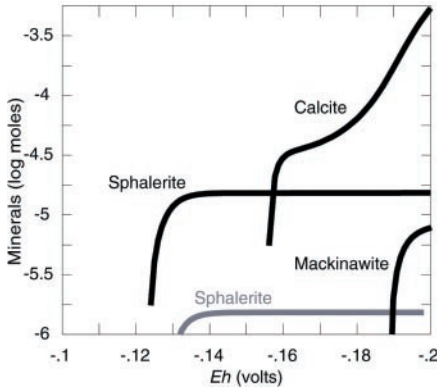

Fig. 6. Diagram mapping the extent of mineral precipitation (vertical axis) as the redox potential decreases from left to right. Black lines show the result for 1 ppm Zn, whereas the gray line shows the result for 0.1 ppm Zn. Sphalerite precipitation greatly precedes the saturation of mackinawite. In the open groundwater flow system, ongoing sphalerite precipitation restricts the accumulation of sulfide and prevents saturation with respect to all iron sulfides.

TEM-based energy-dispersive x-ray analyses showed that SRB cultured in $ZnSO_4$/$FeSO_4$-containing SRB media (*20*) precipitated ZnS but not iron sulfides (*8*). This confirms that geochemical gradients in proximity to cells can lead to saturation with respect to sphalerite without precipitation of iron sulfide, even if iron is present in appreciable concentrations.

Our results demonstrate that coupled geochemical and microbial processes can efficiently strip Zn from solutions with Zn contents of <1 ppm. This process reduces aqueous Zn (and probably As and Se) concentrations to well below acceptable levels for

Table 2. Impurity content in ZnS (wt %) determined by synchrotron-based microprobe analyses. Column [1], results from a 1-μm-diameter aggregate; column [2], average results for four analysis points on other micrometer-scale aggregates.

Ion	[1]	[2]
Mn	0.12	0.103 ± 0.024
Fe	0.20	0.174 ± 0.025
As	0.0096	0.009 ± 0.0032
Se	0.0042	0.0043 ± 0.0018
Ca	0.67	0.902 ± 0.295
K	2.37	4.67 ± 1.28

drinking water. On the basis of the volume of ZnS precipitated in the biofilm, we estimate that the biofilm has concentrated Zn at least 10^6 times relative to the bulk fluid.

There is considerable controversy associated with interpretation of the complex paragenetic sequences responsible for Zn ore deposit formation. Organic geochemical and isotopic indicators of biological sulfate reduction have been reported from some Pb and Zn deposits (*21*, *22*), and microbial precipitation of metastable iron sulfides in sediments is widely accepted. The precipitation process we document is expected to operate under a fairly wide range of temperature conditions and could readily generate mixed metal sulfide assemblages [including galena (PbS) at an Eh of −130 mV in (*8*)] if heterogeneities in sulfide concentration (and thus, Eh) develop (Fig. 6). The process may be relevant to the early stages of formation of the large sediment-hosted deposits from brines, exhalative fluids, or basinal fluids, and to formation of other low-temperature ZnS deposits.

References and Notes

1. M. Ledin, K. Pedersen, *Earth-Sci. Rev.* **41**, 67 (1996).
2. H. L. Ehrlich, *Geomicrobiol. J.* **16**, 135 (1999).
3. L. P. Miller, *Boyce Thompson Inst. Contr.* **16**, 85 (1950).
4. L. G. M. Baas Becking, D. Moore, *Econ. Geol.* **56**, 259 (1961).
5. K. L. Temple, N. LeRoux, *Econ. Geol.* **59**, 647 (1964).
6. W. J. Drury, *Water Environ. Res.* **71**, 1244 (1999).
7. U.S. Environmental Protection Agency, Office of Ground Water and Drinking Water, *Current Drinking Water Standards* (2000).
8. Supplementary data are available at *Science* Online at www.sciencemag.org/cgi/content/full/290/5497/1744/DC1.
9. J. F. Banfield, S. A. Welch, H. Zhang, T. T. Ebert, R. L. Penn, *Science* **289**, 751 (2000).
10. G. W. Luther III, A. L. Meyerson, J. J. Krajewski, R. Hires, *J. Sediment. Petrol.* **50**, 1117 (1980).
11. E. T. Degens, H. Okada, S. Honjo, J. C. Hathaway, *Mineral. Deposita* **7**, 1 (1972).
12. D. K. Newman, D. Ahmann, F. M. M. Morel, *Geomicrobiol. J.* **15**, 255 (1998).
13. D. C. Nelson *et al.*, *Geochem. Cosmochim. Acta.* **60**, 3531 (1996).
14. M. Vainshtein, H. Hippe, R. M. Kroppenstedt, *Syst. Appl. Microbiol.* **15**, 554 (1992).
15. F. Widdel, F. Bak, in *The Prokaryotes*, A. Balows, H. G. Trüper, M. Dworkin, W. Harder, K.-H. Schleifer, Eds. (Springer-Verlag, New York, 1992), pp. 3352–3378.
16. D. Minz *et al.*, *Appl. Environ. Microbiol.* **65**, 4659 (1999).
17. D. Minz *et al.*, *Appl. Environ. Microbiol.* **65**, 4666 (1999).
18. A. Teske *et al.*, *Appl. Environ. Microbiol.* **64**, 2943 (1998).
19. L. G. Benning, R. T. Wilkin, H. L. Barnes, *Chem. Geol.* **167**, 25 (2000).
20. SRB were enriched in modified DSMZ 63-media (DSMZ, Braunschweig, Germany); instead of lactate, pyruvate was used as carbon source, and $FeSO_4$ or $ZnSO_4$ was used as electron acceptor. Subsequently, 10 ml of the $FeSO_4$ media were combined with 50 ml of $ZnSO_4$ media and inoculated with 300 μl of homogenized white biofilm. Incubation occurred anaerobically at ~19°C.
21. M. A. Hu, J. R. Disnar, L. Barbanson, I. Suarez-Ruiz, *Can. J. Earth Sci.* **35**, 936 (1998).
22. G. A. Logan, M. C. Hinman, M. R. Walter, R. E. Summons, *Geochem. Cosmochim. Acta*, in press (2000).
23. W. H. Casey, P. E. Brown, B. F. Jones, S. Golding, and H. L. Ehrlich provided constructive comments. We thank P. Taglia for BTEX analyses; W. W. Barker for sample preparation; K. Meverden, A. Gesell, G. Gormann, R. Polich, and R. Clark for assistance with sampling; and K. W. Germino, J. Maser, Z. Cai, and P. Ilinski for assistance with the x-ray microprobe experiment. Banfield's group acknowledges financial support from the U.S. Department of Energy (DOE) Office of Basic Energy Sciences, NSF Division of Earth Sciences Programs, and the NASA Jet Propulsion Laboratory Astrobiology Institute. The x-ray microprobe analyses carried out at the Advanced Photon Source were supported by the DOE Office of Energy Research, Office of Basic Energy Sciences, and Office of Biological and Environmental Research (NABIR Program) and internal Argonne National Laboratory (LDRD) funds. Support for PEEMS analysis was provided by the Ecole Polytechnique Federale de Lausanne, the Swiss Fonds National de la Recherche Scientifique, and the University of Wisconsin Synchrotron Radiation Center. Electron microscopy was carried out in the Materials Science Center, University of Wisconsin–Madison. G.A.L. and R.E.S. publish with permission of the chief executive of the Australian Geological Survey Organization.

7 August 2000; accepted 6 October 2000

Tropical Climate at the Last Glacial Maximum Inferred from Glacier Mass-Balance Modeling

Steven W. Hostetler[1] and Peter U. Clark[2]

Model-derived equilibrium line altitudes (ELAs) of former tropical glaciers support arguments, based on other paleoclimate data, for both the magnitude and spatial pattern of terrestrial cooling in the tropics at the last glacial maximum (LGM). Relative to the present, LGM ELAs were maintained by air temperatures that were 3.5° to 6.6°C lower and precipitation that ranged from 63% wetter in Hawaii to 25% drier on Mt. Kenya, Africa. Our results imply the need for a ~3°C cooling of LGM sea surface temperatures in the western Pacific warm pool. Sensitivity tests suggest that LGM ELAs could have persisted until 16,000 years before the present in the Peruvian Andes and on Papua, New Guinea.

Fossil pollen and the geologic record showing an ~900-m lowering of equilibrium line altitudes (ELAs) of former tropical glaciers (*1*) have long been used to argue that tropical sea surface temperatures (SSTs) were lower during the last glacial maximum (LGM, 21,000 years ago) than those reconstructed by Climate/Long-Range Investigation, Mapping and Prediction (CLIMAP) project members (*2–6*). Because upper treeline records are possibly compromised by the effects of lower atmospheric CO_2 concentrations at the LGM (*7*), former glaciers are the principal source of high-altitude paleoclimate data in the tropics. Traditionally, paleotemperatures inferred from glacial records have been based on the assumption that lower ELAs were solely the result of temperature changes associated with modern atmospheric lapse rates. Quantifying LGM temperatures that supported lower ELAs on tropical glaciers is complicated, however, by the relative contributions of precipitation (and perhaps net radiation) that also influence the ELA. Moreover, recent analyses of low- and mid-altitude pollen records suggest that tropical atmospheric lapse rates during the LGM may have differed from those of present (*5*), and so the possibility exists that temperature anomalies may have varied with elevation. Uncertainties in the age of maximum ELA depression further complicate inferences of LGM climate made from glacial records (*8–11*).

Here we apply a mass-balance model to several key tropical glaciers to determine the LGM temperature and precipitation climatologies required to produce glaciers in mass balance with surface areas that match those estimated from the geologic record. Baseline LGM temperature and precipitation values used in the glacier model were obtained from simulations conducted with the GENESIS (v. 2.01) atmospheric general circulation model (AGCM). Three multiyear simulations are considered: a present-day simulation with fixed SSTs (control), an LGM simulation in which the CLIMAP SST reconstruction is specified (CLIMAP), and an LGM simulation with an SST field in which lower tropical SSTs than those of CLIMAP are prescribed in the eastern tropical Pacific and equatorial Atlantic Oceans [Oregon State University (OSU)] (*12, 13*). Other than SSTs, the GENESIS simulations were run with standard prescribed boundary conditions (*14*).

Monthly average values of temperature and precipitation from GENESIS were interpolated (*15*) onto a high-resolution (1-km) digital elevation model (DEM) (*16*) that resolves most, but not all, of the topographic

[1]U.S. Geological Survey, Department of Geosciences, Oregon State University, Corvallis, OR 97331, USA. E-mail: steve@ucar.edu. [2]Department of Geosciences, Oregon State University, Corvallis, OR 97331, USA. E-mail: clarkp@ucs.orst.edu